Energy 183 (2019) 525–535

Contents lists available at ScienceDirect

Energy

journal homepage: www.elsevier.com/locate/energy

Influence of cooling architecture on data center power consumption

Hosein Moazamigoodarzi [a, b], Peiying Jennifer Tsai [a], Souvik Pal [a], Suvojit Ghosh [a], Ishwar K. Puri [a, b, *]

[a] Computing Infrastructure Research Centre, McMaster University, Hamilton, Ontario, Canada
[b] Department of Mechanical Engineering, McMaster University, Hamilton, Ontario, Canada

ARTICLE INFO

Article history:
Received 16 November 2018
Received in revised form
24 May 2019
Accepted 21 June 2019
Available online 22 June 2019

Keywords:
Data center
Distributed cooling
Power consumption
Row-based
Rack-based

ABSTRACT

Almost thirty percent of the power consumed by data centers (DCs) is attributable to the cooling of IT equipment (ITE). There are opportunities to reduce a DC's energy budget by considering alternatives to traditional cooling methods, which experience inherent airflow deficiencies due to hot air recirculation and cold air bypass. Minimizing these two air distribution problems results in more effective cooling, but the two effects are manifest differently in the three conventional DC cooling architectures, i.e., (a) room-based, (b) row-based, and (c) rack-based cooling. Despite the intuitive logic that predicts improved cooling air distribution within row- and rack-based architectures that include shorter airflow path-lengths compared to room-based systems that have longer paths, the mechanism through which improvements translate into energy savings is not well understood. Therefore, we present methodologies that resolve the characteristic airflow and temperature distributions for three cooling architectures using computational fluid dynamics. These results inform thermodynamics models of the power consumptions that are required to cool these three architectures. The analysis reveals that row- and rack-based architectures reduce cooling power by much as 29% over a room-based architecture. Adding an enclosure within row- and rack-based architectures to separate the hot and cold airflows provides further 18% reduction in cooling power. This analysis facilitates better DC design from a cooling power consumption perspective.

1. Introduction

The electrical power consumed by the IT equipment (ITE) in a data center (DC) is converted into heat, which must be removed. This heat removal is typically equivalent to almost thirty percent of the power consumed by a DC [1–4]. Although liquids offer significantly higher heat transfer capabilities, most DCs use air cooling due to the simplicity of its application and handling [1–5]. An air-cooled DC can contain thousands of ITE items, each with a cold air inlet and hot air outlet, thereby making airflow distribution inside a DC complex [6]. The design and control of these air paths significantly influences the cooling efficacy.

Air cooling has two major distribution problems, hot air recirculation and cold air bypass [7–9]. When cold air supply to the ITE is insufficient, the hot air exhausted from servers is recirculated to ITE inlets by fans inside the servers, increasing the inlet air temperatures. Bypass occurs when a portion of the cold airflow returns to the cooling unit without contributing to server cooling. While minimizing these air distribution issues leads to more effective cooling, simultaneously reducing the energy consumed for cooling, the two effects manifest differently in the three conventional DC cooling architectures, namely, (a) room-based cooling, where cold air is delivered directly to the room through arrangements such as raised floors and hot air return plenums, (b) row-based cooling, where the cooling unit is located between IT racks or mounted above them so that cold air is delivered to a row of racks, and (c) rack-based cooling, where the cooling unit is integrated entirely within a single IT rack [6,10].

A DC cooling system must accomplish two tasks simultaneously, i.e., (1) remove heat from hot air issuing from the ITE and (2) distribute cold air to it. For room-, row- and rack-based cooling architectures, the first task is identical since the cooling system capacity must match the total power consumed by the ITE. The second task, distribution of cold air to the ITE, is however performed differently for room-, row- and rack-based cooling. Airflow

* Corresponding author. McMaster University, 1280 Main St. W., Hamilton, ON, L8S 4L7, Canada.
E-mail address: ikpuri@mcmaster.ca (I.K. Puri).

https://doi.org/10.1016/j.energy.2019.06.140
0360-5442/

paths are shorter and more predictable for row- and rack-based architectures than for room-based systems since they are isolated from room constraints in the former case.

Despite the intuitive logic that predicts improved airflow distribution with row- and rack-based architectures over room-based systems [6,11], the mechanism of the reduction in cooling energy consumption has not been explained. This analysis is required if DC operators are to make informed decisions while selecting a particular DC designer. The literature related to DC power consumption and cooling optimization that discusses the influence of workload distribution, ITE configurations, cooling unit layouts, aisle separation and containment, and physical dimensions on cooling system efficacy is generally limited to room-based cooling applications [12–25]. These prior investigations do not identify how changing the cooling architecture influences airflow features and the energy consumed by cooling systems.

Studies comparing the benefits of row-based solutions with room-based cooling [6,11] are scarce and only provide qualitative comparisons of the reduction in average air temperature at server inlet and of the return temperature index, both of which are difficult to translate readily in terms of total system energy consumption. Extensions of these results to enclosed rack-based solutions, such as the inclusion of a rack mountable cooling unit (RMCU) within each enclosed IT rack, and comparison with room and row-based architectures are not reported widely in the literature. This lack of guidance is significant considering the rapid emergence of single rack data centers for edge computing, where rack mountable cooling solutions offer a more attractive deployment and maintenance choice. Therefore, we compare the characteristic airflow and temperature distributions for the three, room-, row- and rack-based, cooling architectures using computational fluid dynamics (CFD) simulations that inform thermodynamics models of cooling power consumption.

2. Methodology

We consider a 200 kW DC room that employs air handler units (CRAHs), water to air heat exchangers, fans, valves, and enclosures for which the heat rejection map is shown in Fig. 1. Cold air flow through the servers transfers heat to the CRAHs, cold water flow in the CRAHs extracts heat from the DC room and transfers it to an air-cooled chiller, while the chiller releases the heat to the ambient. There are other possibilities for implementing cooling, e.g., using a water-cooled chiller and cooling tower instead of an air-cooled chiller, or placing the refrigeration cycle inside the DC room in the form of an air conditioner, but these are not considered herein. While the selected configuration may not be the most energy efficient for all possible cases, our purpose is to compare the cooling power consumption by the three different cooling architectures. Such an overall analysis is independent of the specific choice of cooling configuration. Certainly, some of the results would change by considering other cooling strategies like using CRACs instead of CRAHs but considering all possible cooling strategies is not within the scope of a single study. For this reason, we compare the architecture-based power consumption for chilled water-based DCs which are commonly used around the word. Furthermore, regardless of the cooling strategy, whether CRAH or CRAC, two parameters with most influence on the cooling efficiency are the same for different cooling strategies, i.e., (1) the required cold air flowrate and (2) the difference between the cooling unit setpoint and maximum server intake temperature. Even by considering just chilled water based DCs, we are comparing the effect of DC cooling architectures on these two parameters which are not dependent on the type of cooling system (CRAH or CRAC).

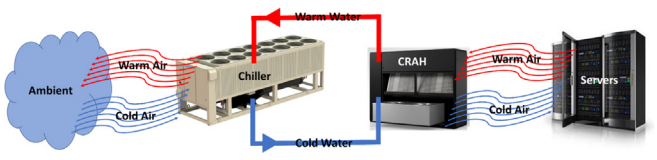

Fig. 1. Heat dissipation route from the heat source to the ambient.

For a selected configuration, the primary energy consuming components include (1) server fans, (2) CRAHs blowers, (3) chilled water pumps and (4) the chiller. Item 1 is similar for the three architectures while item 3 consumes at most 3% of total cooling power [26] so that even for a 30% difference in water pumping power, the difference in total cooling power is less than 1%, which is negligible. Thus, we only compare items 2 and 4 above for room-, row-, and rack-based cooling.

To calculate the energy consumption of the CRAH blowers and the chiller, we must determine (1) total heat rejection from ITEs (assumed to be 200 kW), (2) total CRAH air flowrate and CRAH (3) setpoints, (4) return air temperatures and (5) chilled water flowrates, (6) chilled water temperature entering these CRAHs, and (7) the ambient air temperature. To compare the three cooling architectures, we consider the two scenarios presented in Table 1 with the restriction that all server intake air temperatures are lower than 26.5 °C.

Since the setpoint is specified for scenario 1, the CRAH air flowrates and their return air temperatures are determined using CFD. For scenario 2, the CRAH air flowrate, which is identical for the three architectures, the CRAH setpoints, and their return air temperatures are also determined with CFD. For both scenarios, the chilled water flowrates in the CRAHs and their water inlet temperatures are calculated using the $\varepsilon - NTU$ method by specifying the type and size of the heat exchanger inside these CRAHs. The room-, row-, and rack-based cooling architecture for the DC room case study are shown in Fig. 2. All configurations considered in this section are uncontained and there is no enclosure. The effect of enclosure and containment is considered in the later section.

2.1. CFD simulations

The CFD simulations are performed using ANSYS Fluent with the temperatures and turbulent flow field modeled through the energy equations and the realizable $k-\varepsilon$ model, which is the most commonly used turbulent model in data center modeling [31–36]. A grid independence analysis is performed to ensure the minimum node count required for accuracy. Three meshes, coarse, medium, and fine, are investigated with node count of 1.6 million, 2.3 million, and 4.7 million, respectively. The fine mesh is selected for all the simulations based on the root mean square of the temperature differences for 43 monitoring points to be less than 1 °C [37]. Whereas the IT load is included in the simulation, the heat load of the building, being a small fraction of the IT load, is neglected. The simulation for room-based cooling includes three CRAHs in a DC room that has a raised floor design. Cold air from the CRAHs passes through the underfloor plenum, entering the room through perforated tiles. We are aware of the additional momentum source when modeling perforated tiles [38]. In order to capture it, additional designated zones on top of the tiles with a height usually equaling that of the under-rack gap must be defined. The perforated tiles are modeled as porous zones to account for the resistance without introducing regions with a momentum source. Warm air exiting the servers returns to the CRAHs through the hot air plenum placed above the room. The racks are arranged in four rows. Each row consists of 10 racks with individual heat loads and airflows. The backs of two adjacent rows, from where hot air leaves the servers,

Table 1
The two scenarios use to compare cooling architectures [27–30].

Scenario	CRAH setpoints	CRAH air flowrates	Maximum inlet air temperature of servers
1	Same for three architectures (17 °C)	Different for three architectures	26.5 °C
2	Different for three architectures	Same for three architectures	26.5 °C

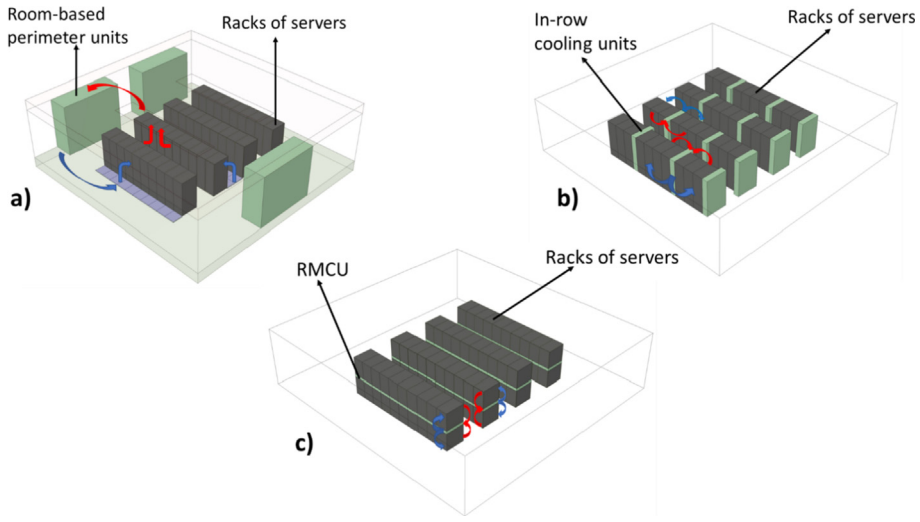

Fig. 2. Geometry of three architectures for the case study DC room: a) room-based, b) row-based, and c) rack-based. All configurations considered in this section are uncontained and there is no enclosure.

are placed facing each other, leading to two hot aisles and three cold aisles. Each rack has an IT load of 5 kW distributed over 20 servers and an airflow rate of 0.39 m^3/s, where each server consumes 0.0195 m^3/s [39]. For row-based cooling, twelve CRAHs are employed in the DC room with three CRAHs per row. The cold air release from the CRAHs flows directly to the cold aisle through their front panels and draw in hot air from the hot aisle through their back panels. For rack-based cooling, each rack is equipped with a single CRAH, resulting in forty CRAHs in the DC room. The CRAHs release cold air directly in front of servers through their front panels and draw in hot air from the backs of the servers through their back panels. For all three cooling architectures, the IT load and airflow are similar for a server rack.

The racks are modeled using a recirculation boundary condition, which employs the first law of thermodynamics to determine the rack exhaust temperature based on a specified heat load and flow rate. Recirculation boundary condition is applicable when a specific amount of heat is removed by a volume that emulates a device whose airflow is known *a priori*. This type of boundary condition is implemented in pairs, i.e., for every recirculation inlet boundary of the domain, there is a recirculation outlet associated with it. The exhaust hot air temperature, which depends on the heating load and flowrate inside the domain as well as the temperature of the cold air supply, is obtained from the CFD simulations. Cooling units are modeled as mass flow inlets and pressure outlets for the cold air supply zones and return air zones, respectively. For the steady-state analysis, cooling air flow rates, rack flow rates, rack heat loads, and supply air temperatures are fixed. Uniform airflows are applied at the rack and cooling unit inlets and outlets to focus on the macroscopic analysis of the different data center cooling architectures. The clearance or gap between the bottom of the rack and the floor may cause air leakages if not properly sealed, and rack manufacturers apply various measures to ensure that this leakage is minimized [40]. Since the geometrical simplification omitting the under-rack gap region has widely accepted [31,32,34–37], we have followed the same approach to perform CFD simulations to conduct like-for-like comparisons. For containments, two-inch gaps between racks with depths equal to those of the racks are considered due to the noticeable pressure differences between the hot and cold containments. These gaps are modeled as porous zones using the power-law model for the resistance,

$$dp = -C_0|v|^{C_1},$$

where dp denotes the pressure drop across the porous zone, $|v|$ the velocity magnitude, and *the* empirical coefficients C_0=*11* and C_1=*1.15* are determined from our experimental results.

To validate the accuracy of the CFD simulations, experiments are performed for one specific configuration [41]. The validation case comprises five IT racks and two in-row cooling units that are contained by an enclosure. The positions of the CRAHs and IT racks, IT load of each rack, CRAH air flowrate and their setpoints are presented in Fig. 3. The deviation of CFD temperature predictions from experimental measurements is defined by $\delta = T_{CFD} - T_{EXP}$. Fig. 4 demonstrates δ for various locations in the front and back chambers, for which the maximum values for the front and back chambers are 0.6 °C and 1.7 °C, respectively. This confirms the relevance and accuracy of the CFD simulations. The higher δ in the back chamber arises due to the obstructing cable bundles there, which are not considered in the simulations.

2.2. Chilled water temperature and flowrate

After determining the air flowrate, supply air temperature, and return air temperature for each CRAH from the simulations, the chilled water characteristics, e.g., water flowrate and water inlet temperature can be calculated. CRAHs contain an air to water heat exchanger to extract the heat from the warm air. To calculate the required water flowrate and inlet temperature, the sizes of the heat exchangers, types of heat exchangers, and characteristics of heat

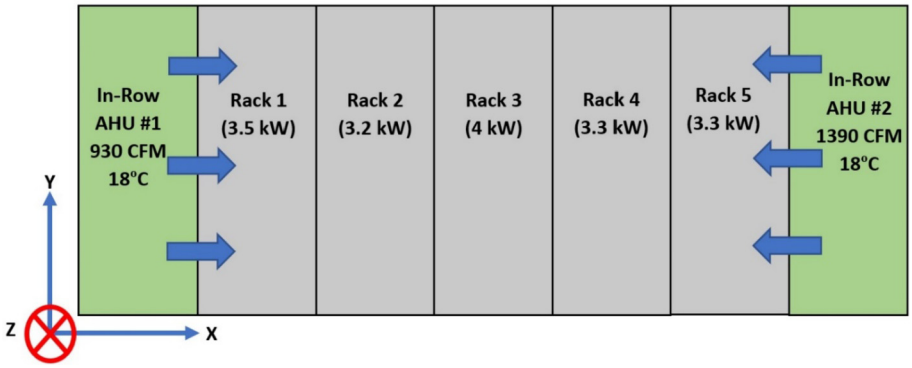

Fig. 3. Configuration of the validation case (front view), including two CRAHs and five IT racks, IT load of each rack, air flowrate of the CRAHs and their setpoints.

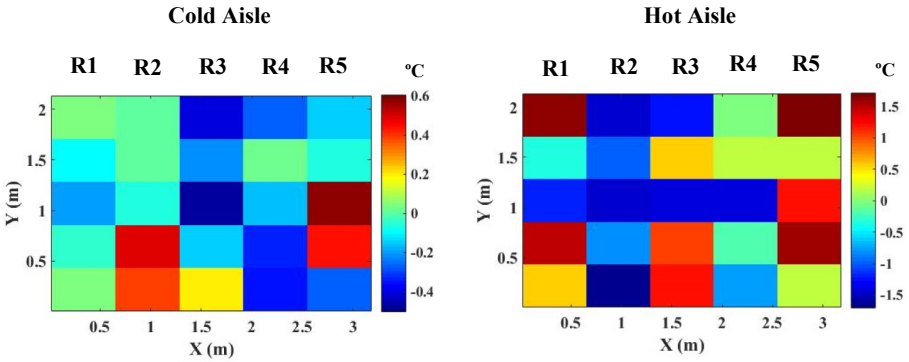

Fig. 4. The values of δ at different locations in the front and back chambers.

exchanger fins must be known. Since optimization of heat exchanger size and fins for CRAHs would greatly increase the complexity of this study, we use fin characteristics and the sizes of heat exchangers that are currently available in the market. The required steady state water flowrate and inlet temperature are calculated using the $\varepsilon - NTU$ method. Heat exchanger details, such as size, fin type and water flowrate, are presented in Table 2. The water flowrate is specified based on available cooling units and the water inlet temperature is calculated with the $\varepsilon - NTU$ method [42,43].

2.3. Power consumption

The power consumed by the refrigeration system in the chiller is a function of the heat load at its evaporator, the temperature of fluid entering the condenser, the desired set point temperature of the water leaving the evaporator, and other operating and design parameters including the loading of the chiller with respect to its rated capacity. While there are several analytical models available in the literature to characterize chiller operation, the Gordon–Ng model is selected for its simplicity and ease since readily available data can fit model coefficients. The Gordon–Ng model has the form [26],

$$y = a_1 x_1 + a_2 x_2 + a_3 x_3, \text{ where} \tag{1}$$

$$x_1 = T_{co}/Q_c, \tag{2}$$

$$x_2 = (T_{ci} - T_{co})/(T_{ci} \times Q_c), \tag{3}$$

$$x_3 = ([(1/COP) + 1] \times Q_c)/T_{ci}, \text{ and} \tag{4}$$

$$y = [(1/COP) + 1] \times (T_{co}/T_{ci}) - 1. \tag{5}$$

The COP, or coefficient of performance, is the ratio of the evaporator heat load to the electrical power consumption by the compressor, T_{ci}, and T_{co} denote the water temperatures in units of K entering the condenser and leaving the evaporator, respectively, and the chiller heat load expressed in kW is Q_c. Data for Q_c, COP, T_{ci}, and T_{co} are obtained from manufacturer test information for a 200 kW chiller [46] for the chiller model,

$$y = 0.05x_1 + 84.31x_2 + 0.072x_3. \tag{6}$$

Equation (6) allows us to determine the compressor power consumption once the total cooling load, evaporator temperature

Table 2
Heat exchanger characterization [44,45].

Architecture	Heat exchanger type	Heat exchanger size (m^3)	Water flowrate (m^3/s)
Room-based	Finned-tube with *louvered fins*	0.20 × 1.50 × 2.25	0.0032
Row-based	Finned-tube with *louvered fins*	0.20 × 0.70 × 2.00	0.0009
Rack-based	Plate-fin with *straight fins*	0.35 × 0.30 × 0.12	0.0004

and condenser temperature are known.

Based on commercially available CRAHs, fans are selected for the three architectures, details for which are presented in Table 3. Manufacturer information is available for fan curves and fan power consumption in the form of data sheets that provide relations between power consumption, pressure drop, and air flowrate. The pressure drop across the heat exchanger inside the CRAHs can be determined based on the fin characteristics, air flowrate, heat exchanger size, and pressure drop correlations. Thereafter, using the fan data sheets, the total power consumption of the fans can be calculated.

3. Results and discussion

3.1. Airside parameters

The air flowrates required and the average return air temperatures for all cases are calculated from the CFD simulations and presented in Table 4. The results presented in this section are for uncontained architectures. For scenario 1, changing the architecture from room-to rack-based, the airflow required of the CRAHs decreases by 50% because the cold air path from the cooling unit to the ITE is shortened. The respective path lengths are (A) ~10 m, (B) ~1 m and (C) ~0.1 m. For case A-1, the air flowrate of the CRAHs should be increased to remove hot spots and maintain the inlet temperatures for all servers lower than 26.5 °C. Distributed cooling architectures (B-1 and C-1) require lower cold air flowrates.

For the second scenario, moving from room-to rack-based cooling allows the CRAH setpoint to increase by 5 °C. Since distributed cooling architectures require lower cold air flowrates, maintaining the same air flowrate for all architectures results in an oversupply of cold air for cases B-2 and C-2. This extra air flowrate produces higher pressures at server inlets than at their exhausts, eliminating recirculation. This increases bypass and produces a more uniform temperature profile in front of servers, eliminating undesirable hot spots, allowing higher CRAH setpoints, thus reducing cooling cost. Fig. 5 demonstrates the differences in the required air flowrates and setpoints for the three cooling architectures.

Recirculation and bypass either lower or raise the air flowrate. Bypass occurs when a portion of the cold air exiting the cooling unit does not reach the servers. For instance, in open space, i.e., with no containment, the cold airflow from the cooling unit can be assumed to have the form of a jet [50]. If the jet does not expand significantly, it reaches the servers without entrainment, but this is of course not the case in practice. The more the entrainment the greater the bypass. The jet entrainment is a function of Re^{-1} [50]. For jet flow, an effective dimensionless number reflecting the amount of bypass is $\sqrt{\mu/\rho \overline{V} L}$, where ρ and μ are the density and dynamic viscosity of air respectively, $\overline{V}$ the jet velocity exiting the cooling unit, and L the distance from the jet source. We realize that this is an approximation since the cold airflow of the cooling unit can be considered as a jet only for open spaces with no containment.

In addition to jet entrainment, the bypass is influenced by the ratio of the mass flowrate through the cooling unit $\dot{m}_{CU}$ and that through the servers $\dot{m}_{IT}$. The higher the value of $\dot{m}_{CU}$, the higher the bypass because there is more cold airflow that is not drawn by the ITEs. However, as $\dot{m}_{IT}$ increases, the ITEs draw more airflow, lowering bypass. The second dimensionless ratio influencing bypass is therefore $\dot{m}_{CU}/\dot{m}_{IT}$.

The third ratio includes the influence of geometry. As air travels from the cooling unit to the ITEs, the longer the distance L, the greater the possibility that the flow deviates in the form of bypass from a desired path. The cross section of the server inlets is the target destination for the cold air stream. Thus, as server inlet cross section area are enlarged, the lower the bypass. Accordingly, the geometric dimensionless ratio is L^2/A_{IT}.

The fourth factor influencing bypass is the angle α between the normal vectors orthogonal to the cooling unit exhaust and the server inlet. When the cooling unit and servers are placed face to face in front of one another, $\alpha = \pi$ and bypass is minimized. The dimensionless angle between these normal vectors is assumed to have the form $\theta = (\alpha + 2k\pi)/(2k\pi + \pi)$, where k denotes a positive integer. Here, k is a tool to control the magnitude of changes of θ when α changes. This ensures that the influence of changes in θ does not surpass the influence of changes in other factors discussed above. We arbitrarily select a desirable value of $k = 2$. When the cooling unit and servers are placed in front of each other, this dimensionless angle equals unity and lower values indicate increasing misalignment between the cooling unit and servers.

In order to present a dimensionless number which can represent the influence of all of these parameters on bypass, we combine the above four dimensionless factors, i.e.,

$$B = \sqrt{\frac{\mu}{\rho \overline{V} L}} \times \frac{\dot{m}_{CU}}{\dot{m}_{IT}} \times \frac{L^2}{A_{IT}} \times \frac{(\pi + 2k\pi)}{(\alpha + 2k\pi)} \tag{7}$$

Lower values of B, which is inversely proportional to $Re = \mu/(\rho \overline{V} L)$ imply lower bypass. If the cooling unit exhaust is placed in front of the server entrance, or $L = 0$ and $\alpha = \pi$, there is no bypass. Bypass increases by increasing $\dot{m}_{CU}/\dot{m}_{IT}$. Changing the architecture from room-to rack-based cooling reduces B because L is considerably shortened. Other dimensionless indices are available in the literature, e.g., return heat index (RHI), rack cooling index (RCI), and recirculation index (RI), but all of these are based on the effect of recirculation and bypass and not on the cause of these effects [51–54]. Moreover, while these indices are based on the temperature distribution within the DC room, which in fact results from recirculation and bypass, Eq. (7) represents the causes of these phenomena.

Recirculation occurs when part of the hot air exiting the servers does not reach the cooling unit. It depends on $\dot{m}_{CU}$, $\dot{m}_{IT}$, cross section area of the cooling unit inlet A_{CU}, distance between the cooling unit inlet and server exhausts L', angle between the normal vectors orthogonal to the cooling unit entrance and the servers exhaust α', velocity of the jet emerging from the servers $\overline{V'}$, and ρ and μ. By applying the above methodology, the dimensionless number characterizing recirculation,

$$R = \sqrt{\frac{\mu}{\rho \overline{V'} L'}} \times \frac{\dot{m}_{IT}}{\dot{m}_{CU}} \times \frac{L'^2}{A_{CU}} \times \frac{(\pi + 2k\pi)}{(\alpha' + 2k\pi)} \tag{8}$$

Again, R is inversely proportional to Re. The lower the value of R

Table 3
Fan characteristics [47–49].

Architecture	Number of fans per CRAH	Fan type	Section area (m^2)	Maximum air flowrate (m^3/s)
Room-based	3	EC backward curved	0.630 × 0.630	4.25
Row-based	5	EC backward curved	0.255 × 0.255	0.57
Rack-based	3	DC, Axial	0.130 × 0.130	0.24

Table 4
Calculated air flowrates and temperatures by CFD for three architectures under two scenarios are presented.

Case	Scenario	Architecture	CRAH setpoint (°C)	CRAH air flowrate (m^3/s)	Maximum air temperature at server's intake (°C)	Average return air temperature to the CRAHs (°C)
A-1	1	Room-based	17	26.6	26.5	23.4
B-1	1	Row-based	17	18.8	26.5	26.3
C-1	1	Rack-based	17	13.4	26.5	29.8
A-2	2	Room-based	15	18.8	26.5	24.3
B-2	2	Row-based	17	18.8	26.5	26.3
C-2	2	Rack-based	20	18.8	26.5	29.4

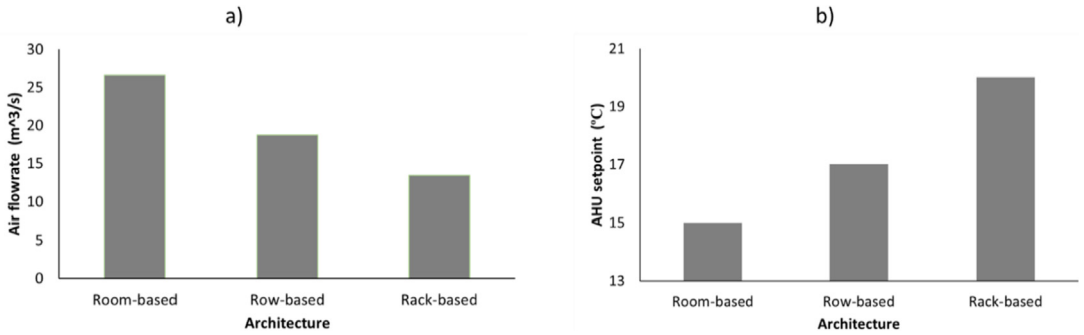

Fig. 5. Comparison of the required air flowrate and setpoint to maintain the inlet air temperature of all the servers lower than 26.5 °C for the cases reported in Table 4. (a) Scenario 1 for same setpoints but different air flowrates. (b) Scenario 2 for same air flowrates but different setpoints.

the lower is the recirculation, but R increases with decreasing $\dot{m}_{CU}/\dot{m}_{IT}$, denoting the challenge for reducing bypass and recirculation simultaneously. Changing from room-to rack-based cooling reduces R because L' is shortened. Values of B and R for all six cases are reported in Table 5. To analyze the relative importance of R and B on energy consumption, we examine their influence on the CRAH air flowrate and setpoint, the two primary determinants of power consumption, as shown in Fig. 6.

3.2. Chilled water

The temperature of the chilled water entering the CRAHs, required to calculate chiller power consumption, is a function of the total heat transfer rate, return air temperature, supply air temperature or setpoint, air flowrate and water flowrate. Since these parameters are known, the water inlet temperature is calculated using the $\varepsilon - NTU$ method. The chilled water characteristics of the three cooling architectures are presented in Table 6.

For scenario 1, even though all cases have the same setpoint, the distributed cooling architectures implemented for cases B-1 and C-1 transfer heat with warmer chilled water, leading to lower cooling costs. Because the number of CRAHs required in distributed architectures is larger, this results in a higher total chilled water flowrate, improving cooling efficacy. Hence, the water inlet temperature can be increased, reducing chilling energy cost. For scenario 2, the water inlet temperature is different due to two reasons. First, the CRAHs have different setpoints which influence the required water inlet temperature and, second, the total water flowrates and heat exchanger types for the three architectures are different. To increase the efficacy of a room-based architecture and reduce cooling cost, one solution is to increase the required chilled water temperature by increasing the total water flowrate. However, there is a limit on the water flowrate inside a heat exchanger, particularly its piping loop.

3.3. Power consumption

Based on Eq. (6) and Table 3, the power consumption of the chiller and the fans for the three cooling architectures are presented in Fig. 7. For scenario 1, cases B-1 and C-1 provide up to 29% reduction in power consumption over case A-1. The rack-based architecture has the best efficacy. For all cooling solutions, the largest contribution to the power consumption is from the compressor in the chiller refrigeration cycle. For scenario 1, moving from room-to rack-based cooling, chiller power consumption decreases because the required water inlet temperature increases. The power consumption by fans for case A-1 is significantly higher than for other architectures because they must provide a higher 26.6 m^3/s air flowrate compared to cases B-1 and C-1 for which the flowrates are respectively 18.8 and 13.4 m^3/s. Although case C-1 has a lower air flowrate compared to case B-1, a similar amount of power is consumed in both cases because fan efficiencies measured as the volume flow per unit energy consumption decrease with a reduction in fan size [55–57]. For the same air flowrates, rack-

Table 5
Bypass number B and recirculation number R.

Case	Scenario	Architecture	CRAH setpoint (°C)	CRAH air flowrate (m^3/s)	B ($\times 10^9$)	R ($\times 10^4$)
A-1	1	Room-based	17	26.6	37	85
B-1	1	Row-based	17	18.8	25	45
C-1	1	Rack-based	17	13.4	5	18
A-2	2	Room-based	15	18.8	32	93
B-2	2	Row-based	17	18.8	25	45
C-2	2	Rack-based	20	18.8	6	11

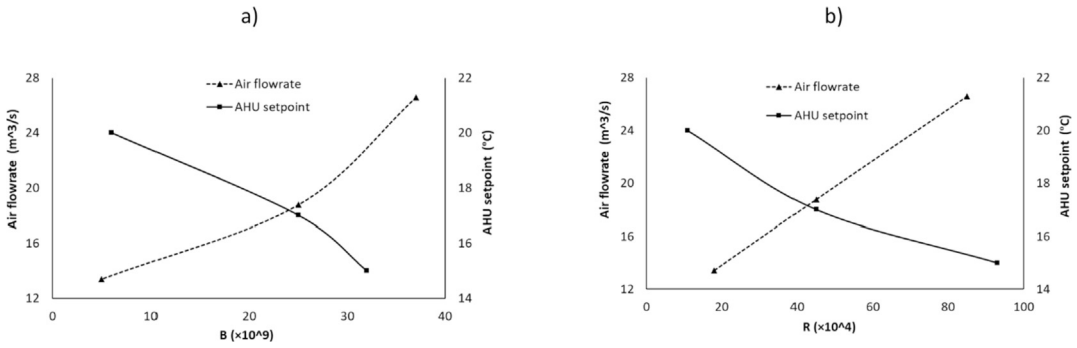

Fig. 6. Influence of Bypass Number B and Recirculation Number R on the required CRAH air flowrate and setpoint. These two parameters are the primary determinants of power consumption.

Table 6
Chilled water characterization of three cooling architectures.

Case	Scenario	Architecture	CRAHs setpoint (°C)	CRAHs air flowrate (m^3/s)	Water temperature entering the CRAHs (°C)	CRAHs water flowrate (m^3/s)
A-1	1	Room-based	17	26.6	7.4	0.0032
B-1	1	Row-based	17	18.8	9.8	0.0009
C-1	1	Rack-based	17	13.4	13.7	0.0004
A-2	2	Room-based	15	18.8	6.5	0.0032
B-2	2	Row-based	17	18.8	9.8	0.0009
C-2	2	Rack-based	20	18.8	16.5	0.0004

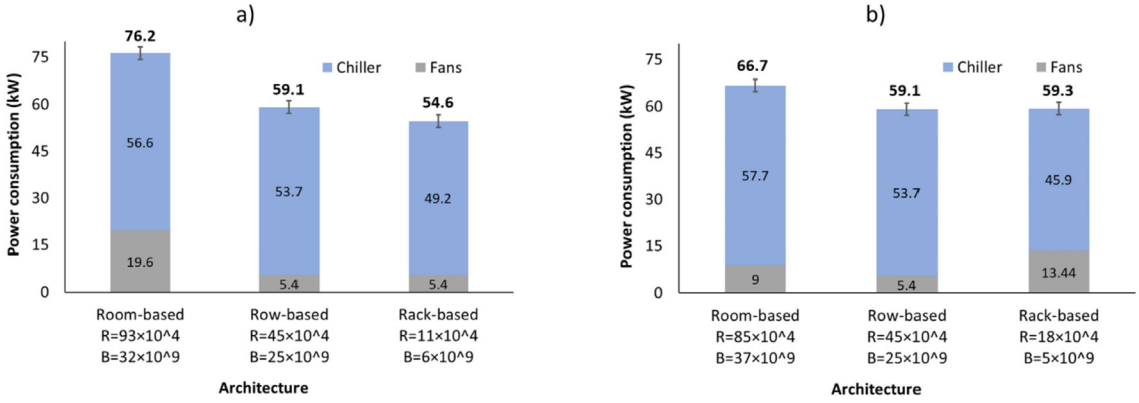

Fig. 7. Comparison of power consumption for the three cooling architectures described in Table 6. (a) Scenario 1 for the same setpoints but different air flowrates. (b) Scenario 2 for the same air flowrates but different setpoints. The values of *R* and *B* for each case are presented to demonstrate their relative influence on power consumption.

based fans consume more power due to their smaller sizes. Furthermore, the size limitation of rack-based CRAHs leads to the requirement for a deeper heat exchanger. The pressure drop across it is consequently higher, resulting in a higher fan power consumption to draw in a specified air flowrate.

For scenario 2, cases B-2 and C-2 provide up to 12% reduction in the power consumption as compared to case A-2. The row-based architecture has the best efficacy. The differences in chiller power consumption for this second scenario are higher because the setpoints of the CRAHs are different and required water inlet temperatures, i.e., 6.5, 9.8, and 16.5 °C, are markedly different for the three room-, row- and rack-based cooling architectures. Besides, fan power consumption for case C-2 is higher due to the use of smaller fans.

3.4. Effect of containment

Containment isolates the hot air exhaust of the ITE from its cold air intake, providing an additional benefit for reducing recirculation regardless of architecture. Therefore, a distributed cooling architecture with containment is expected to be the most energy efficient configuration. We examine the power consumption of enclosed room-, row- and rack-based cooling to understand the influence of enclosures that separate the hot and cold airflows on power consumption. The geometries of the enclosed row- and rack-based cooling architectures for a case study DC room are shown in Fig. 8. For the row and rack-based architectures, we assume that the front and back chambers are separated by placing dense commercially available brushes in gaps, which are modeled in Ansys Fluent as a porous media. While there are various methods for separating the hot and cold airflows for room-based architecture, we select "hot aisle containment" since it is a common configuration for room-based architectures [58–61].

The required air flowrates and setpoints for all architectures are presented in Fig. 9. For Scenario 1, the required air flowrates for all three architectures are lower. Here, since the front and back chambers are separated, both recirculation and bypass are minimized. For the required airflowrate, the rack-based solution uses

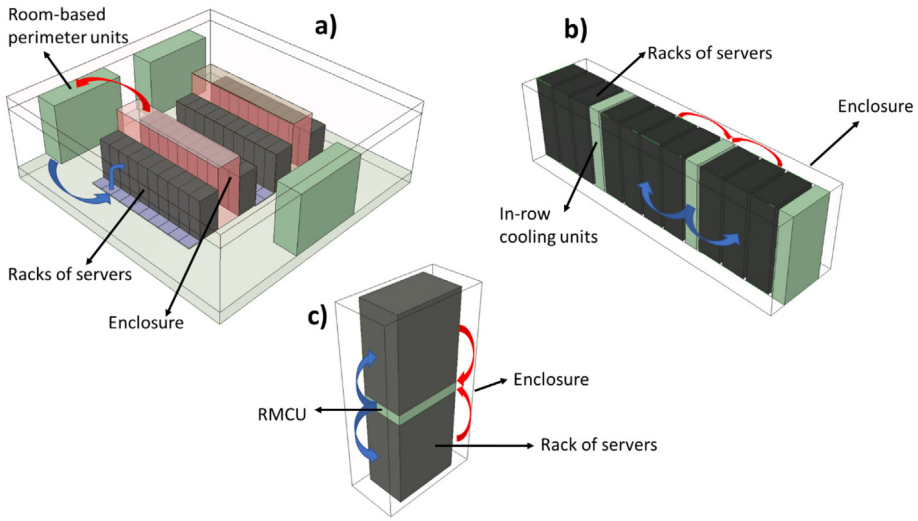

Fig. 8. Geometry of three architectures that include enclosures for a case study DC room: (a) room-based architecture, (b) row-based architecture, and (c) rack-based architecture.

the minimum (12.5 m^3/s) while the room-based solution requires the maximum amount (15 m^3/s). Adding an enclosure reduces the required air flowrate by 46% for the room-based, 24% for the row-based and 8% for the rack-based cooling architecture compared to their values for open architecture. So, the maximum reduction in required air flowrate by adding containment is observed for room-based architectures.

By using an enclosure for scenario 2, the CRAH setpoint for all three architectures are improved. Adding enclosures that separate the chambers reduces recirculation and bypass resulting in more uniform temperature profiles in the front chamber and diminishing hotspot formation. Therefore, the difference between the setpoint temperature and the maximum server intake temperature decreases so that then the CRAH setpoint can be at a higher temperature. The rack-based solution has the highest setpoint (25.3 °C) while the room-based solution has the lowest setpoint (22 °C). The CRAH setpoints for room-, row- and rack-based architectures can be maintained at an additional 7, 8 and 5 °C higher, respectively compared to their values for open architecture.

To compare the three architectures, regardless of their cooling unit characteristics, such as fan size and heat exchanger type, we examine just the flowrates and setpoints shown in Fig. 9. In general, we can conclude that, based on airflow characteristics, the rack-based architecture is best for eliminating bypass and recirculation. Comparing the power consumption required by these three architectures, we must consider their cooling units characteristics, which are different for each type of CRAH.

In essence, an enclosure that separates chambers reduces power consumption because of a lower required air flowrate and higher CRAH setpoint. The power consumption for all cases that are considered is presented in Fig. 10. The best solution for Scenario 1 is rack-based cooling with an enclosure, while for Scenario 2 it is the row-based architecture within an enclosure. However, the rack-based cooling architecture could have the best efficacy for energy consumption if more energy efficient smaller fans were to become available.

We note that the power consumption calculations for the room- and row-based architectures are general and valid for common room- and row-based solutions, but the corresponding calculation for the rack-based architecture is valid only for rack mountable cooling units. We have selected rack mountable cooling units for the rack-based architecture for the following reasons: (1) This is the only rack-based solution which can fit within an isolated IT cabinet. Other possible rack-based configurations, such as rear door cooling, require air transfer to the room. Our motivation for the study is based on our interest in modular data centers, which do not allow

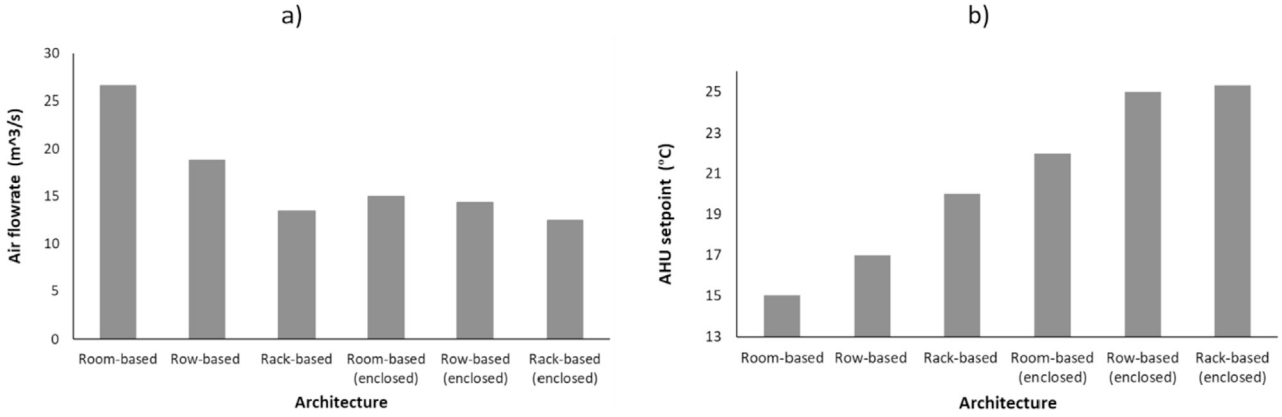

Fig. 9. Comparison of air flowrates and setpoints for enclosed architectures with the open architectures for two scenarios. (a) Scenario 1 for same setpoints but different air flowrates. (b) Scenario 2 for same air flowrates but different setpoints.

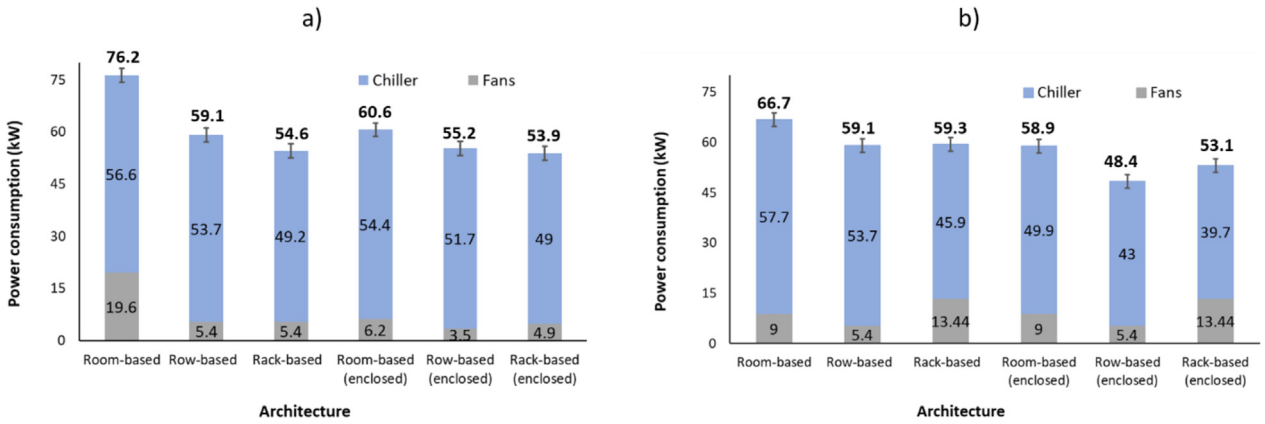

Fig. 10. Comparison of power consumption for enclosed architectures with the open architectures for two scenarios. (a) Scenario 1 for the same setpoints but different air flowrates. (b) Scenario 2 for the same air flowrates but different setpoints.

any air transfer to the room. (2) Since our research is translational, our commercial collaborator (CINNOS) produces rack mountable cooling units. To be immediately helpful to industry, our intention is to compare the rack mountable solution with other cooling architectures. (3) The rack mountable cooling unit is a new solution for modular data centers. While not yet common, it has the potential for wider future use since it helps further overcomes the space limitations that make modular data centers desirable.

The dimensionless numbers presented in the previous section ***B*** and ***R*** are applicable for open environments, where jet-like airflows dominate, but not for enclosed environments. However, when there is containment, momentum is a lesser factor since there is a pressure driven flow through the resistances [62,63]. A simplified mechanical resistance circuit for DCs with containment is illustrated in Fig. 11. Obviously, this simplified circuit cannot represent all flow patterns of an enclosed DC, but it does show the basic flow for the three architectures with containment. The description of each resistance is provided in the figure caption.

If the air flows through the paths $R_2 \rightarrow R_3 \rightarrow R_4 \rightarrow R_5$, there is no bypass and recirculation, but if there is any airflow through R_1 there will be either bypass or recirculation. If the airflow through R_1 is from the cold chamber to the hot chamber, there is bypass and if it is from the hot chamber to the cold chamber, there is recirculation. By increasing the quality of separation between the chambers by increasing R_1, the amount of bypass and recirculation are reduced. Essentially, for enclosed DCs, the ratio $(R_2+R_3+R_4+R_5)/R_1$ determines the intensity of bypass and recirculation. The implication of Fig. 11 is that the rack-based architecture has lowest $(R_2+R_3+R_4+R_5)/R_1$ while the room-based architecture has the highest.

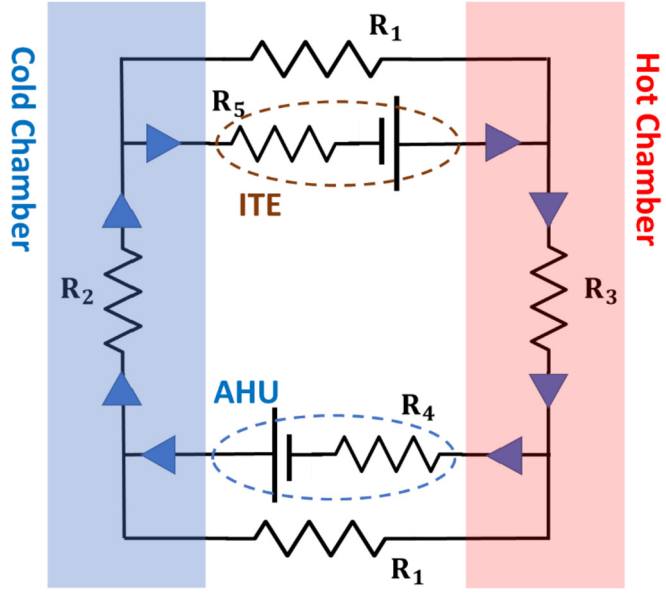

Fig. 11. Simplified mechanical resistance circuit for DCs with containment. R1: The mechanical resistance due to the separation between the cold and hot chambers. R2: The mechanical resistance between the CRAH outlet and the ITE inlet. R3: The mechanical resistance between the ITE outlet and the CRAH inlet. R4: The mechanical resistance across the CRAH, mainly due to the heat exchanger. R5: The mechanical resistance across the ITE. The two power supplies are the fans inside the CRAH and the ITE.

4. Conclusion

We compare the power consumption of three DC cooling architectures. Row- and rack-based distributed cooling architectures are more energy efficient as compared to the conventional room-based architecture. Adding enclosures within distributed cooling architectures reduces their cooling cost further. These energy savings occur due to significant reductions in recirculation and bypass.

We find that, (1) for a constant temperature setpoint, distributed cooling architectures require up to a 50% lower cold air flowrate, (2) for constant airflow, distributed cooling architectures increase the CRAH setpoint by as much as 5 °C, (3) the dimensionless number B representing bypass decreases to one-seventh for the rack-based configuration as compared to room-based cooling, (4) the dimensionless number R representing recirculation decreases to one-ninth for rack-based cooling as compared to its value for the room-based configuration, (5) distributed cooling architectures enable an increase in the water temperature entering the CRAHs by 6 °C, (6) row- and rack-based architectures facilitates a 29% reduction in cooling power consumption, and (7) adding an enclosure within the distributed cooling architecture results in an additional 18% energy savings.

Beside improving energy efficiency, distributed cooling architectures, both row- and rack-based, have lower initial cost and are more easily maintained, with greater agility and manageability. Considering all of the above aspects, employing enclosed distributed cooling architectures is the best choice from a DC energy consumption perspective.

Acknowledgment

This research was supported by the Natural Sciences and Engineering Research Council of Canada under a collaborative research and development (CRD) project titled: Adaptive Thermal Management of Data Centers. We also thank our colleagues from CINNOS Mission Critical Incorporated who provided insight and expertise that greatly assisted the research.

References

[1] Dai J, Ohadi MM, Das D, Pecht MG. Optimum cooling of data centers, application of risk assessment and mitigation techniques. New York: Springer Science Business Media; 2014. https://doi.org/10.1007/978-1-4614-5602-5.
[2] Ebrahimi K, Jones GF, Fleischer AS. A review of data center cooling technology, operating conditions and the corresponding low-grade waste heat recovery opportunities. Renew Sustain Energy Rev 2014;31:622–38.
[3] Daraghmeh HM, Wang CC. A review of current status of free cooling in datacenters. Appl Therm Eng 2017;114:1224–39.
[4] El-Sayed N, Stefanovici IA, Amvrosiadis G, Hwang AA, Schroeder B. "Temperature management in data centers: why some (might) like it hot," *Sigmetrics '12*, no. TECHNICAL REPORT CSRG-615. 2012. p. 163–74.
[5] Patterson MK. "The effect of data center temperature on energy efficiency," *2008 11th IEEE Intersoc*. Conf Therm Thermomechanical Phenom Electron Syst I-THERM 2008:1167–74.
[6] Dunlap K, Rasmussen N. Choosing between room, row, and rack-based cooling for data centers. Schneider Electr. White Pap. 2012;130:18.
[7] Cho J, Kim BS. "Evaluation of air management system's thermal performance for superior cooling efficiency in high-density data centers. Energy Build 2011;43(9):2145–55.
[8] Cho J, Yang J, Park W. "Evaluation of air distribution system's airflow performance for cooling energy savings in high-density data centers. Energy Build 2014;68:270–9. PARTA.
[9] Patankar SV. Airflow and cooling in a data center. J Heat Transf 2010;132(7). 073001.
[10] N. Rasmussen, "The different types of air distribution for IT environments", White paper 55, APC By Scenider Electric.
[11] Huang Z, Dong K, Sun Q, Su L, Liu T. Numerical simulation and comparative analysis of different airflow distributions in data centers. Procedia Eng. 2017;205:2378–85.
[12] Pakbaznia E, Pedram M. Minimizing data center cooling and server power costs. Proc. 14th ACM/IEEE Int. Symp. Low power Electron. Des. - ISLPED 2009;09:145.
[13] Nada SA, Said MA. Effect of CRAC units layout on thermal management of data center. Appl Therm Eng 2017;118:339–44.
[14] Song Z, Zhang X, Eriksson C. Data center energy and cost saving evaluation. Energy Procedia 2015;75:1255–60.
[15] Lyu C, Chen G, Ye S, Liu Y. Enclosed aisle effect on cooling efficiency in small scale data center. Procedia Eng. 2017;205:3789–96.
[16] Rong H, Zhang H, Xiao S, Li C, Hu C. Optimizing energy consumption for data centers. Renew Sustain Energy Rev 2016;58:674–91.
[17] Hamann H, Iyengar M, O'Boyle M. "The impact of air flow leakage on server inlet air temperature in a raised floor data center," *2008 11th IEEE Intersoc*. Conf. Therm. Thermomechanical Phenom. Electron. Syst. I-THERM 2008: 1153–60.
[18] Bhopte S, Agonafer D, Schmidt R, Sammakia B. Optimization of data center room layout to minimize rack inlet air temperature. J Electron Packag 2006;128(4):380.
[19] Cho K, Chang H, Jung Y, Yoon Y. Economic analysis of data center cooling strategies. Sustain. Cities Soc. 2017;31:234–43.
[20] Habibi A, Halgamuge SK. "A Review on efficient thermal management of air- and liquid-cooled data centers : from chip to the cooling system. Appl Energy 2017;205:1165–88. March.
[21] Patel CD, Shah AJ. Cost model for planning, vol. 107. Development and Operation of a Data Center; 2005. p. 1–36. *Development*.
[22] Capozzoli A, Primiceri G. Cooling systems in data centers: state of art and emerging technologies. Energy Procedia 2015;83:484–93.
[23] Beitelmal AH, Patel CD. Thermo-fluids provisioning of a high performance high density data center. Distributed Parallel Databases 2007;21(2–3): 227–38.
[24] Sharma RK, Bash CE, Patel CD, Friedrich RJ, Chase JS. Balance of power: dynamic thermal management for internet data centers. IEEE Internet Comput. 2005;9(1):42–9.
[25] Silva-llanca L, Ortega A, Fouladi K. Determining wasted energy in the airside of a perimeter-cooled data center via direct computation of the Exergy Destruction. Appl Energy 2018;213:235–46. January.
[26] Iyengar M, Schmidt R. Analytical modeling for thermodynamic characterization of data center cooling systems. J Electron Packag 2009;131(2). 021009.
[27] Pelley S, Meisner D, Wenisch TF, Van Gilder JW. Understanding and abstracting total data center power. In: Workshop on energy efficient design. WEED); 2009.
[28] Schmidt R. Effect of data center characteristics on data processing equipment inlet temperatures. In: Proc. ASME pacific rim technical conf. And exhibition on integration and packaging of MEMS, NEMS, and electronic systems collocated with the ASME heat transfer summer conf.; 2001. p. 1097–106.
[29] Schmidt R, Iyengar M. Effect of data center layout on rack inlet air temperatures. In: Proc. ASME pacific rim technical conf. And exhibition on integration and packaging of MEMS, NEMS, and electronic systems collocated with the ASME heat transfer summer conf.; 2005. p. 517–25.
[30] ASHRAE TC9.9 mission critical facilities, technology spaces, and electronic equipment, thermal guidelines for data processing environments, American society of heating. Refrigeration, and Air-conditioning Engineers, Inc.; 2011. http://tc99.ashraetcs.org.
[31] Fulpagare Y, Bhargav A. Advances in data center thermal management. Renew Sustain Energy Rev 2015;43:981–96.
[32] Abdelmaksoud WA, Khalifa HE, Dang TQ, Schmidt RR, Iyengar M. "Improved CFD modeling of a small data center test cell," *2010 12th IEEE Intersoc*. Conf. Therm. Thermomechanical Phenom. Electron. Syst. 2010:1–9.
[33] Buratti C, Palladino D, Moretti E. Prediction of indoor conditions and thermal comfort using CFD simulations: a case study based on experimental data. Energy Procedia 2017;126:115–22.
[34] Durand-Estebe B, Le Bot C, Mancos JN, Arquis E. Data center optimization using PID regulation in CFD simulations. Energy Build 2013;66:154–64.
[35] Hassan NMS, Khan MMK, Rasul MG. Temperature monitoring and CFD analysis of data centre. Procedia Eng. 2013;56:551–9.
[36] Gao C, Yu Z, Wu J. Investigation of airflow pattern of a typical data center by CFD simulation. Energy Procedia 2015;78:2687–93.
[37] Cruz E, Joshi Y. Inviscid and viscous numerical models compared to experimental data in a small data center test cell. J Electron Packag 2013;135(3). 030904.
[38] M. Seymour, S. Davies, "What is a valid data center model? An introduction to calibration for predictive modeling", Future Facilities' White Paper FFL-007 Revision 1.0.
[39] Moazamigoodarzi H, Pal S, Ghosh S, Puri IK. Real-time temperature predictions in IT server enclosures. Int J Heat Mass Transf 2018;127:890–900.
[40] Wan J, Gui X, Kasahara S, Zhang Y, Zhang R. Air flow measurement and management for improving cooling and energy efficiency in raised-floor data centers: a survey. IEEE Access 2018;6:48867–901.
[41] Abdelmaksoud WA, Khalifa HE, Dang TQ, Elhadidi B, Hall L. "Experimental and computational study of perforated floor tile in data centers,". In: 12th IEEE intersoc. Conf. Therm. Thermomechanical Phenom. Electron. Syst.; 2010. p. 1–10.
[42] Shah RK, Sekulic DP. Fundamentals of heat exchanger design. John Wiley & Sons; 2003.
[43] Hochsteiner E, Segundo DV, Levati A, Cocco V, Coelho S. Thermodynamic optimization design for plate- fi n heat exchangers by Tsallis JADE. Int J Therm Sci 2017;113:136–44.
[44] Product Data Sheet, *RITTAL*, CRAC Precision climate control units for data centres. 2014. Model Number:3300.387.
[45] Product data sheet, *RITTAL*, TopTherm LCP rack/inline CW. vol. 530; 2015. Model Number: 3311.130/3311.
[46] Product data sheet, *YORK*, air-cooled scroll chillers with brazed plate heat exchangers, style: E, model: YCAL.
[47] Product Data Sheet, *ebm-papst* , EC centrifugal fan. 2012. Model Number: R3G250-RO40-A9.
[48] Product data sheet, *ebm-papst* , EC centrifugal fan RadiPac. 2016. Model Number: R3G450-PI86 -01.
[49] Product data sheet, *delta electronics, inc*, model number: THD1348HE, specification for approval. 2017.
[50] Kundu PK, Cohen IM, Dowling DR. Fluid mechanics, fifth edit. Academic Press is an imprint of Elsevier; 2016.
[51] Hoseyni SM, Norouzi-Khangah B, Mohammadsadeghi-Azad MB, Hoseyni SM. Performance assessment of cooling systems in data centers; Methodology and application of a new thermal metric. Case Stud. Therm. Eng. 2016;8:152–63.
[52] Herrlin MK. Rack cooling effectiveness in data centers and telecom central offices: the Rack Cooling Index (RCI). ASHRAE Transact 2005;111(2):725–31.
[53] Tozer R, Kurkjian C, salim M. "Air management management metrics in Data Centers" *ASHRAE*. 2009. CH-09-009.
[54] VanGilder J, Shrivastava S. "Capture Index: an airflow-based rack cooling performance metric " *ASHRAE*, DA-07-014. 2007.
[55] Mathson T, Ivanovich M. AMCA ' s fan efficiency Grades : answers to frequently asked questions. AMCA International 2011. www.amca.org.
[56] A closer look at fan eficciency Look", providing insights for today's HVAC system designer. Engineering Newsletter 2014;43 –3. Trane.
[57] AMCA standard 205 , energy efficiency rating for fans. Technical news, BULLETIN; 2014. 30.
[58] J. Niemann, K. Brown, and V. Avelar "Impact of hot and Cold aisle containment on data center temperature and efficiency", White paper 135, APC By Scenider Electric.
[59] Xu Y, Gao Z. "Analyzing the cooling behavior of hot and cold aisle containment in data centers," fourth. Int. Conf. Emerg. Intell. Data Web Technol. 2013;(2011):685–9.
[60] Zhou R, Wang Z, Bash CE, Mcreynolds A. Modeling and control for cooling management of data centers. USA: Proceedings of the ASME International Mechanical Engineering Congress & Exposition; 2011.
[61] Schmidt R, Vallury A, Iyengar M. "ENERGY savings through hot and cold aisle

containment configurations for," proceedings of the asme pacific rim technical conference & exposition on packaging and integration of electronic and photonic systems. 2011 [USA].
[62] VanGilder J, Shrivastava S. A flow-network model for predicting rack cooling in containment systems. In: Proceedings of the ASME InterPACK conference; 2009 [USA].
[63] Vangilder JW. A hybrid flow network-CFD method for achieving any desired flow partitioning through floor tiles of a raised-floor data center. 2019. p. 1–6.